Lattice Boltzmann scheme for fluids with dynamic heterogeneities

A. Lamura

Istituto Applicazioni Calcolo, CNR, Sezione di Bari, Via Amendola 122/D, 70126 Bari, Italy

S. Succi

Istituto Applicazioni Calcolo, CNR, V.le del Policlinico 137, 00161 Roma, Italy

We introduce and discuss a three-dimensional mesoscopic lattice Boltzmann model for the numerical simulation of strongly-interacting fluids with dynamic inhomogeneities. The model is based on an extension of the standard lattice Boltzmann dynamics in which streaming between neighboring lattice sites is constrained by the value of the nonlocal density of the surrounding fluid. The resulting dynamics exhibits typical features of dynamically heterogeneous fluids, such as long-time relaxation, non-Gaussian density distributions and dynamic heterogeneities. Due to its intrinsically parallel dynamics and absence of statistical noise, the method is expected to compute significantly faster than molecular dynamics, Monte Carlo, and lattice glass models.

I. INTRODUCTION

Understanding the microscopic origins of sluggish relaxation, long-time equilibration, and dynamical heterogeneities in complex fluids, such as supercooled liquids, polymers, and other glassylike materials, is one the most challenging frontiers of current condensed matter research [1,2]. A number of powerful and elegant theoretical approaches have been developed in the recent past to tackle the aforementioned problems, such as mode coupling theory (MCT) [3] and the multidimensional landscape picture [4]. However, none of these theoretical approaches provides a fully comprehensive picture of long-time relaxation in complex fluids, so that there is still a great need for computer simulations. The numerical study of slowly-relaxing complex fluids is usually undertaken by many-body simulation methods, such as molecular dynamics [5], Monte Carlo [6], and various types of lattice "glasses" [7–12]. Although many-body methods have the potential to explain complex-fluid behavior *ab initio*, this potential remains largely unrealized for want of computational power. Since many-body simulations are computationally so demanding, there is a constant need of exploring whether the basic features of slowly-relaxing fluids can be reasonably described by effective one-body techniques, in the spirit of density functional theory [13]. A powerful one-body technique which has recently gained significant momentum for the study of complex interacting fluid flows is the lattice Boltzmann (LB) method. This method is based on the stylized dynamics of fictitious molecules which move along the links of a regular lattice, and at each lattice site interact according to a local collisional relaxation dynamics.

The LB dynamics consists of three basic steps: (i) free streaming, (ii) collisional relaxation [14], and (iii) intermolecular interactions [15]. Free motion (kinetic energy) drives the system out of equilibrium, while collisional relaxation tends to restore it, within the typical time scale of binary (hard core) collisions, τ_c. For weakly interacting fluids, potential energy is usually small compared to kinetic energy, so that the effect of (soft core) intermolecular interactions can be reabsorbed into a properly generalized local equilibrium, typically a local Maxwellian with a shifted local speed u

$\rightarrow u + a\tau_c$, where a is the acceleration associated with the intermolecular potential $V(r)$. A suitable choice of the intermolecular interactions $V(r)$ permits to describe the dynamics of a variety of complex flows [16]. However, applicability of LB to *strongly*-interacting and glassylike fluids remains an open problem [17], which has only recently received a plausible LB formulation [18]. This paper contains a more detailed and enlarged presentation of the model recently published in Ref. [18]. Distinctive features of the physics of complex fluids are geometrical frustration and resulting dynamic heterogeneities. This means that the presence of sterical constraints reduces the phase space available to the fluid system and prevents binary collisions to restore local equilibrium within the short-time collisional scale τ_c. As a result, fluids develop dynamic inhomogeneities which relax on a time scale, τ, much larger than the collisional one, τ_c. In other words, the system performs plenty of ineffective collisions which do not contribute to relax the density contrasts. Pictorially, a slowly-relaxing fluid can be viewed as a collection of homogeneous subdomains, each characterized by its own local relaxation time scale. Real systems such as colloids, or granular materials, exhibit glassy dynamics associated to jamming: Density increase, rather than temperature decrease, is the dominant mechanism responsible for the dramatic slowing down of the system dynamics [19]. The lattice Boltzmann equation (LBE) with density constraints presented here aims at representing geometric frustration and sterical constraints by confining the free-particle motion to a dynamic subset of links which fulfill self-consistent constraints on the surrounding fluid density. The presence of these kinetic constraints on the free particle motion leads to drastic departures from simple fluid behavior, such as long-time relaxation, dynamic heterogeneities and non-Gaussian density fluctuations.

II. THE MODEL

A. LBE for simple diffusion in ideal fluids

We begin by considering the standard LBE in single-time relaxation form [20,21]

$$f_i(\mathbf{r},t) - f_i(\mathbf{r}_i, t - \Delta t) = -\omega \Delta t [f_i - f_i^e](\mathbf{r}_i, t - \Delta t), \quad (1)$$

where $f_i(\mathbf{r},t) \equiv f(\mathbf{r}, \mathbf{v} = \mathbf{c}_i, t)$ is the probability of finding a fluid particle at site $\mathbf{r}$ and time t, moving along the direction i of a lattice, with a discrete speed $\mathbf{c}_i$, where $c_i = \Delta x / \Delta t$.

In the above Δx and Δt are the lattice space and time steps, respectively, obeying the light-cone condition $\mathbf{r}_i \equiv \mathbf{r} - \mathbf{c}_i \Delta t$. The latter condition implies that the particles are grid bound, i.e., they live on the nodes of the space-time lattice. The LBE results from the combination of two competing mechanisms: Free-streaming and collisional relaxation. In the collision step, the distribution functions f_i relax to a local equilibrium f_i^e in a time lapse of the order of ω^{-1}. As a result, the distribution function after a collision f_i^c is

$$f_i^c(\mathbf{r}_i, t - \Delta t) = f_i(\mathbf{r}_i, t - \Delta t) - \omega \Delta t [f_i - f_i^e](\mathbf{r}_i, t - \Delta t). \quad (2)$$

The free streaming moves the post-collisional distributions to the neighboring sites pointed by the discrete speeds $\mathbf{c}_i$. The distribution function f_i^c then streams freely to neighbor sites, so that the updated values are just the shifted post-collisional distributions

$$f_i(\mathbf{r},t) = f_i^c(\mathbf{r}_i, t - \Delta t). \quad (3)$$

The large-scale behavior of the system depends crucially on the form of the local equilibria. In the present work, the equilibrium distribution functions f_i^e are expressed as

$$f_i^e(\mathbf{r},t) = w_i \rho(\mathbf{r},t), \quad (4)$$

where w_i is a set of lattice-dependent weights normalized to unity, the lattice analog of the global Maxwell distribution in the continuum. This is at odd with standard LBE where f_i^e depend on fluid velocity [21]. In this case we are interested in considering convective effects. In the following, we shall refer to a three-dimensional cubic lattice of size $L \times L \times L$ with six nearest-neighbor connections, $\mathbf{c}_i = (\pm \Delta x / \Delta t, 0, 0)$, $(0, \pm \Delta x / \Delta t, 0)$, $(0, 0, \pm \Delta x / \Delta t)$, $i = 1, 2, \ldots, 6$, plus a rest particle with zero speed $\mathbf{c}_0 = (0,0,0)$. The equilibrium weights for this lattice are $w_0 = 1/3$ and $w_i = 1/9$ for $i = 1, 2, \ldots, 6$. The local density $\rho(\mathbf{r}, t)$ in Eq. (4) is obtained by a direct summation upon all discrete distributions

$$\rho(\mathbf{r},t) = \sum_i f_i(\mathbf{r},t). \quad (5)$$

Since the local equilibria do not depend on the local fluid speed, the only conserved quantity is the fluid density. This means that in the continuum limit, the system obeys a simple diffusion equation $\partial_t \rho(\mathbf{r},t) = D\nabla^2 \rho(\mathbf{r},t)$, with diffusion coefficient

$$D = c_s^2 \Delta t \left(\frac{1}{\omega \Delta t} - \frac{1}{2} \right), \quad (6)$$

where $c_s = \frac{\Delta x}{\sqrt{3}\Delta t}$ is the sound speed. This result can be derived as follows. Let us consider the LBE in semidiscrete form (only the velocity degrees of freedom are left discrete)

$$\partial_t f_i + c_{ia} \partial_a f_i = \omega(f_i^e - f_i). \quad (7)$$

In the above, subscripts denote Cartesian components, which are notationally convenient for algebraic manipulations of

tensorial quantities, and repeated indices are summed upon. Upon summing over all discrete speeds ($\Sigma_i \cdots$), the LBE delivers the continuity equation

$$\partial_t \rho + \partial_a J_a = 0, \quad (8)$$

where

$$J_a(\mathbf{r},t) = \sum_i c_{ia} f_i(\mathbf{r},t) \quad (9)$$

is the current density. By taking weighted averages over the discrete speeds ($\Sigma_i \mathbf{c}_i \cdots$), we obtain the evolution equation for the current density (momentum equation)

$$\partial_t J_a + \partial_b P_{ab} = -\omega J_a, \quad (10)$$

where

$$P_{ab}(\mathbf{r},t) = \sum_i c_{ia} c_{ib} f_i(\mathbf{r},t) \quad (11)$$

is the momentum-flux tensor. On the right hand side of (10), we have taken into account the fact that the equilibrium distribution does not contribute to the fluid current. By applying ∂_t to (8), ∂_a to (10), and summing up, we obtain

$$\partial_{tt} \rho + \omega \partial_t \rho = \partial_a \partial_b P_{ab}. \quad (12)$$

This has the form of a telegrapher's equation, which still contains the same amount of information as the semidiscrete LBE. Next come two essential near-equilibrium approximations. First, we assume the system evolves slowly on a time scale $\tau_c \equiv 1/\omega$ (*adiabatic approximation*), so that the term $\partial_{tt} \rho$ can be neglected. Second, we assume that, on the same time scale, the momentum flux tensor is basically enslaved to its equilibrium form, $P_{ab} \simeq P_{ab}^e = \rho c_s^2 \delta_{ab}$, where the latter equality stems directly from the specific form of the equilibrium distribution (4). Combination of the adiabatic and near-equilibrium approximations finally delivers the promised diffusion equation

$$\partial_t \rho = c_s^2 \tau_c \partial_a^2 \rho, \quad (13)$$

with a diffusivity $D = c_s^2 \tau_c$. The missing $-1/2$ factor in the diffusivity is due to the fact that the semidiscrete LBE was derived from the LBE by a first-order Taylor expansion of the discrete streaming operator. However, a consistent Chapman-Enskog treatment of the LBE requires a second-order Taylor expansion, from which the factor $-1/2$ can be readily derived [22]. It is worth noting that within the present kinetic formalism, diffusion is not represented by second-order spatial derivatives, but rather *emerges* as an adiabatic limit of a first-order propagation-relaxation dynamics. The practical advantage from the computational viewpoint, is that the diffusive Courant-Friedrichs-Levy condition for numerical stability, $D\Delta t < \Delta x^2$, is replaced by the advective condition, $c\Delta t \leq \Delta x$. This means that the time-step scales only linearly rather than quadratically with the mesh spacing.

B. LBE with dynamical density constraints

Sterical constraints have proven very effective in capturing the physics of glassy systems, where density is the domi-

nant observable [2,10]. Kinetic constraints on the evolution of the system are enforced within the LB formalism by the following functional rule: *Propagation from a site* **r** *to any of its six neighbors* **r**′ *is permitted only if the nonlocal densities prior and after streaming, both lie below a given density threshold, S.* In equations

$$\rho_{nl}(\mathbf{r}) \equiv \sum_{i=1}^{6} \rho(\mathbf{r} + \mathbf{c}_i \Delta t) < S, \tag{14}$$

$$\hat{\rho}_{nl}(\mathbf{r}') \equiv \sum_{i=1}^{6} \hat{\rho}(\mathbf{r}' + \mathbf{c}_i \Delta t) < S, \tag{15}$$

where the caret indicates quantities *after* a (tentative) streaming step.

In the limit $S \to \infty$, streaming is free and the effective propagator taking a particle from site **r** at time t to site **r**′ at time $t + \Delta t$, reduces to the standard free-particle form, $G_i(\mathbf{r}, \mathbf{r}'; \Delta t) = \delta(\mathbf{r}' - \mathbf{r} - \mathbf{c}_i \Delta t)$. In the opposite limit, $S \to 0$, no motion is allowed and $G_i \to \delta(\mathbf{r}' - \mathbf{r})$ at all sites, corresponding to structural arrest. Therefore, the ratio

$$\lambda = 6\langle\rho\rangle/S \tag{16}$$

where $(\langle \cdots \rangle$ stands for spatial average and six is the number of neighbors), is a measure of the strength of nonlinear interactions and controls the transition from the purely diffusive to the structural arrest regime. In the absence of an underlying microscopic theory, the density threshold S is to be treated as a free parameter, actually the only one, of our model. The above functional rule is implemented via the following algorithm:

(1) *Initialization:* Initialize the system by setting N randomly chosen lattice sites at a local density ρ_0 and the remaining $L^3 - N$ ones at a density 0. The average density in the system is then $\langle\rho\rangle = \chi\rho_0 \leq \rho_M$, where $\rho_M = \rho_0$ is the maximum possible average density in the system, and $\chi = N/L^3$ is the concentration of "loaded" sites;

(2) *Compute local equilibria:* Compute the local densities $\rho(\mathbf{r})$ via Eq. (5) and the equilibrium distribution functions f_i^e via Eq. (4);

(3) *Collision:* Perform the collision (2) at all the lattice sites to compute f_i^c;

(4) *Check density constraints for prestreaming:* Look for *all* the lattice sites $\mathbf{r}^*$ such that $\Sigma_{i=1}^{6}\rho(\mathbf{r}^* + \mathbf{c}_i \Delta t) < S$, where S is the selected density threshold;

(5) *Prestreaming:* According to Eq. (3), the post-collide populations f_i^c computed at step 3 are propagated *only* along links emanating from the lattice sites **r** and pointing towards neighbor sites $\mathbf{r}^*$;

(6) *Check density constraints for actual streaming:* Compute again local densities $\hat{\rho}(\mathbf{r})$ at *all* the lattices sites. Look for *all* the lattice sites $\mathbf{r}^{**}$ such that $\Sigma_{i=1}^{6}\hat{\rho}(\mathbf{r}^{**} + \mathbf{c}_i \Delta t) < S$;

(7) *Streaming:* Perform the effective streaming step of the f_i^c computed at step 3 only along links from $\mathbf{r}^*$ to $\mathbf{r}^{**}$ sites (these links will be denoted as *active* ones), otherwise the f_i^c do not move;

(8) *Go to 2.*

It is worth noting that the present scheme differs considerably from current LB models for nonideal fluids. Indeed, while the latter include nonideal effects through (effective) potential energy interactions which leave the free-particle propagator (kinetic energy) unaffected, in our case the interactions are so intense to possibly block off the free-particle trajectories. This is typical of strongly interacting systems in which potential energy cannot be treated as a perturbation to kinetic energy. Formally, weakly interacting fluids can be described by an effective Hamiltonian of the form $H = p^2/2m + V[\rho]$, where $V[\rho]$ is a weakly nonlocal functional of the density field. For instance, in the popular Shan-Chen model [23], one has $V[\mathbf{r}, \mathbf{r}_i] = G\Psi(\rho(\mathbf{r}))\Psi(\rho(\mathbf{r}_i))$, where $\Psi(\rho)$ is a suitable "generalized density," implementing attractive/repulsive potential energy interactions depending on the sign of the coupling constant G. In our case, the kinetic constraints can be conveyed into a renormalized mass, $m[\rho]$, such that the effective velocity $v[\rho] = p/m[\rho]$ takes on the values 1 and 0 (in lattice units) depending on whether or not the density field complies with the dynamical constraints. As a result, the present LBE extension can be viewed as a discrete analog of a one-body effective kinetic equation of the form

$$\partial_t f + \mathbf{v}[\rho] \cdot \nabla f = \omega(f^e - f), \tag{17}$$

where the notation $\mathbf{v}[\rho]$ indicates that the particle speed is a nonlinear and nonlocal functional of the density field

$$v[\rho] = \Phi(S - \rho_{nl}(\mathbf{r}))\Phi(S - \hat{\rho}_{nl}(\mathbf{r}')), \tag{18}$$

where $\Phi(\cdot)$ denotes the Heavyside function. To the best of these authors' knowledge, this equation appears to be new in the framework of strongly inhomogeneous fluids.

III. SIMULATION RESULTS

We have simulated two lattice sizes, $L = 16$ and $L = 32$, in lattice units $\Delta x = \Delta t = 1$. The lattice fluid is initialized at a constant density $\rho = \rho_0$ in the N loaded sites, and $\rho = 0$ in the $L^3 - N$ unloaded ones. Periodic boundary conditions are used. The relaxation frequency ω has been varied in the range $[0.1 : 1]$ without finding any dependence of the results on its specific value. Thus, we set $\omega = 0.1$, corresponding to a collisional relaxation time $\tau_c = 10$, and to a kinematic diffusivity $D = 3.16$ (in lattice units). At a given value of the initial density ρ_0, we choose the smallest value of S such as to ensure sluggish dynamics at high densities, while still allowing the system to attain a uniform steady state at low densities. The natural measure for the strength of nonlinear interactions is given by the parameter λ in Eq. (16). This is also the basic parameter controlling the transition from the purely diffusive to structural arrest regimes, through the intermediate of sluggish relaxation.

A. Transition from diffusive to structural arrest regime

By running several simulations with $\rho_0 = 0.5$, we have found that for $S \gtrsim 1$ the system evolves through diffusive smoothing of the density gradients towards a long-time state characterized by a uniform density when $\langle\rho\rangle \lesssim 0.03$. More-
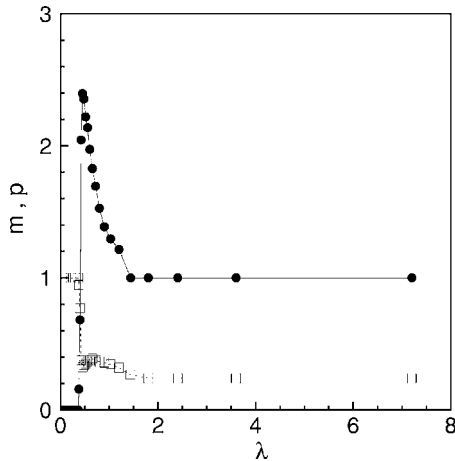
FIG. 1. The order parameter m ($\bullet$) and the participation number p ($\square$) as a function of the reduced density λ with $\rho_0=0.5$, $\langle\rho\rangle=0.12$, and $L=32$.

FIG. 2. Autocorrelation function $h(t)$ as a function of time t for $\langle\rho\rangle=0.08$ ($\triangle$), 0.09 ($\bigcirc$), 0.10 ($\star$), 0.11 ($\bullet$), 0.12 (*), 0.18 ($\diamond$), 0.30 ($\square$) with $\rho_0=0.5$, $S=1.5$, and $L=32$.

over, when $S\gtrsim 2.3$, the system does not show any singular behavior for densities smaller than the maximum possible one, ρ_M (see below). This latter feature is also observed by increasing ρ_0 while keeping $S=1.5$. This is because, by increasing ρ_0 at a fixed average density $\langle\rho\rangle$, the number N of lattice sites to be initialized with density ρ_0 decreases, and consequently the kinetic constraints are less effective. Summarizing, we have used $\rho_0=0.5$ and $S=1.5$, corresponding to single site density threshold $\rho_S=S/6=0.25$. For this set of parameters, the system is seen to exhibit a nonsmooth transition from diffusive to sluggish behavior as the reduced density is increased. This is shown in Fig. 1, where we plot the order parameter

$$m = (\rho_{max} - \rho_{min})/\rho_0, \qquad (19)$$

as a function of λ. In the above, ρ_{max} and ρ_{min} are the maximum and minimum values of ρ, respectively, at steady state. These data are obtained by keeping $\langle\rho\rangle=0.12$ and $\rho_0=0.5$ fixed and varying S. The values of m were averaged over 50 independent runs on systems of size $L=32$. The simulations yield $m\simeq 0$ for $\lambda\lesssim 0.36$, indicating a purely diffusive behavior, then m undergoes a sharp rise and the system enters the sluggish regime. At values of $\lambda\gtrsim 1.44$, the system is nearly frozen in its initial configuration and the order parameter m settles down to 1 since $\rho_{max}=\rho_0$ and $\rho_{min}=0$. Figure 1 indicates the existence of three distinct regimes, namely a low-density diffusive regime at $\lambda<\lambda_D\simeq 0.36$, a high-density frozen regime at $\lambda>\lambda_F\simeq 1.44$, and a sluggish regime at intermediate densities $\lambda_D<\lambda<\lambda_F$. Since the initial density of occupied sites is ρ_0, the initial nonlocal density $\rho_{nl}(\mathbf{r})=\sum_{i=1}^{6}\rho(\mathbf{r}+\mathbf{c}_i\Delta t)$ can be at most $6\rho_0$. Therefore, the condition for a purely diffusive behavior is $6\rho_0\lesssim S\Rightarrow\lambda\lesssim 0.24$, which is in a reasonable agreement with the value provided by simulations. The value of λ marking the transition from the glassy to the frozen regime can be determined by considering that the average initial nonlocal density is $\rho_{nl}(\mathbf{r})=6\chi\rho_0$. When $6\chi\rho_0\gtrsim S\Rightarrow\lambda\gtrsim 1.0$, the system is likely to be frozen. This underestimates the value obtained from simulations, but the value of the order parameter $m(\lambda=1)\simeq 1.3$, well below
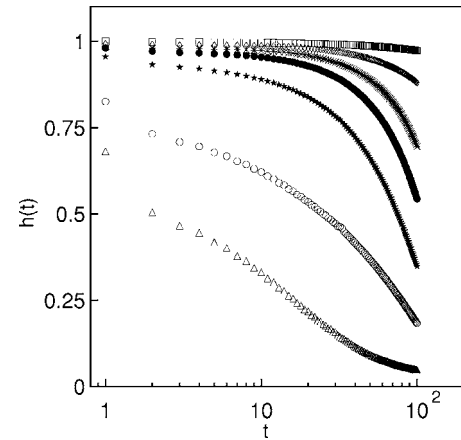
its maximum $m\simeq 2.4$, indicates that the system is approaching the frozen regime. In the following, we fix $\lambda=0.48$, in order to select a regime with a clear departure from ideal fluid behavior ($m(\lambda=0.48)\simeq 2.35$). For this set of parameters the system evolves from the initial random configuration forming some clusters until, at long times, it gets arrested in one of the highly heterogeneous states. The arrest time decreases with increasing average density $\langle\rho\rangle$, as we shall detail shortly. Also shown in Fig. 1 is the steady-state value of participation number p, defined as $p=1/(L^3\sum_{i=1}^{L^3}p_i^2)$, with $p_i=\rho(\mathbf{r}_i)/(\chi L^3\rho_0)$ being the occupation probability of the site i. By definition $p(t=0)=\chi$ and $p=1$ in the case of uniform distribution (least localization). This plot shows that $\chi<p<1$ indicating that the system never becomes more localized than in the initial configuration.

B. Long-time relaxation: The autocorrelation function

We computed the time autocorrelation function

$$h(t) = \frac{\langle\langle \delta\rho(t+t_0)\delta\rho(t_0)\rangle\rangle}{\langle\langle \delta\rho(t_0)\delta\rho(t_0)\rangle\rangle}, \qquad (20)$$

where $\langle\langle\cdots\rangle\rangle$ denotes an average over space and initial times t_0 and $\delta\rho(t)=\rho(t)-\langle\rho\rangle$ is the density fluctuation. The plots for several values of the initial density $\langle\rho\rangle$ are shown in Fig. 2 for the case $L=32$. Data were obtained by averaging over 50 independent runs for each value of $\langle\rho\rangle$. For very small values of $\langle\rho\rangle$, the system goes to a final state with uniform density and $h(t)$ relaxes to zero. By increasing $\langle\rho\rangle$, $h(t)$ starts forming a plateau and stays close to the unit value for a time span which increases rapidly with increasing mean density $\langle\rho\rangle$. Even at high densities, the correlator does not exhibit the "two-step" relaxation behavior often found in glassy materials. This is probably due the absence of a rattling motion in our model [a similar behavior is found in the Kob-Andersen (KA) model [7] for lattice glasses]. We compared our results with the predictions of MCT [3] that predicts a power-law time decay away from the plateau. Therefore, we fitted the short-time behavior of the function $h(t)$ with a power law of
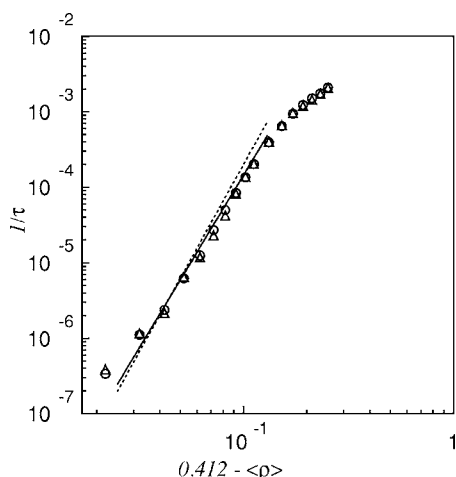
FIG. 3. Inverse relaxation time $1/\tau$ as a function of $0.412-\langle\rho\rangle$ for $\rho_0=0.5$, $S=1.5$, and $L=16$ ($\triangle$), 32 ($\bigcirc$). The full line has slope 4.68. For a comparison we plotted the results of the KA model by using a dashed line.

FIG. 4. Fraction F of active links as a function of $0.471-\langle\rho\rangle$ for $\rho_0=0.5$, $S=1.5$, and $L=16$ ($\triangle$), 32 ($\bigcirc$). The full line has slope 4.19. For a comparison we plotted the results of the KA model by using a dashed line.

the form $f-Bt^b$, where f, B, and b are fitting parameters. Such a power-law decay is indeed reproduced by our simulations in the high-density regime, where the whole set of fits yield f very close to 1 (to within 10^{-3}) as in the KA model [7]. The coefficient B decreases at increasing values of $\langle\rho\rangle$ varying in the range $[4\times10^{-5}:3\times10^{-4}]$. At variance with MCT predictions, the power-law exponent b is not independent of density but decreases at increasing values of $\langle\rho\rangle$ varying in the range $[0.8:1.0]$. This density dependence of b is found also in the KA model [7] with b decreasing at increasing values of $\langle\rho\rangle$ varying in the range $[0.8:1.1]$, which is consistent with our results. In MCT the decay at longer times is predicted to be a stretched exponential, $h(t) \propto \exp[-(t/\tau)^\beta]$, where the exponent β is density independent and the relaxation time τ is the relevant physical parameter. Indeed, this time scale increases strongly as density is increased (MCT predicts a singular behavior for τ at a density smaller than the maximum one ρ_M). Chemically different materials relax in a qualitatively similar manner with relaxation functions obeying the Kohlraush-William-Watts function $\exp[-(t/\tau)^\beta]$ [24]. We fitted successfully $h(t)$ at long times for $\langle\rho\rangle\gtrsim0.12$ by using the stretched exponential with τ and β as fitting parameters and found that the inverse relaxation time $1/\tau$ vanishes at a critical density $\rho_c=0.412\pm0.010$, with power law $6(\rho_c-\langle\rho\rangle)^{\gamma_c}$, being $\gamma_c=4.68$ (in the KA model [7] the critical exponent γ_c is ~5), while the stretching exponent β is density dependent. MCT predicts such a power law behavior for the relaxation time with a system-dependent exponent γ_c [25]. We stress that the critical value ρ_c is smaller than the maximum density ρ_M, corresponding to a fully-loaded lattice. The plot of the relevant physical quantity $1/\tau$ as a function of $\rho_c-\langle\rho\rangle$ is shown in Fig. 3, where we also report the fitting values of $1/\tau$ for the system size $L=16$. Also in this case, we found that $1/\tau$ vanishes with a power-law behavior and the estimated critical density is 0.405 ± 0.029, which is consistent with ρ_c within the error range, with no significant lattice size effect. This suggests a singular behavior at about $\langle\rho\rangle=0.412$. It is to be
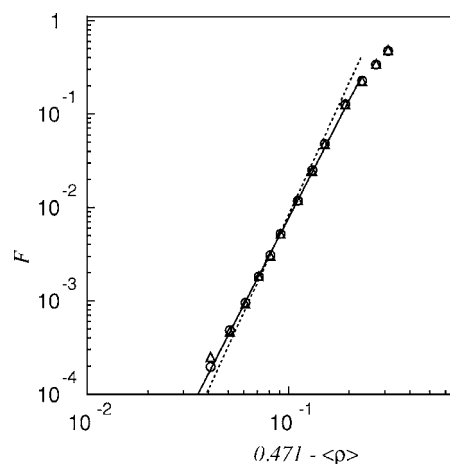
noted that our data show a six orders of magnitude increase of the relaxation time over the microscopic, collisional value, $\tau_c=10$.

C. Fraction of active links and effective potential energy

We also inspected the ratio F of active lattice links to the total number $6L^3$ of lattice links. This quantity can be viewed as a measure of the degree of "congestion" or glassiness, as observed in kinetically constrained lattice glass models [12]. In the limit $\langle\rho\rangle\rightarrow0$, $F\rightarrow1$ since the kinetic constraints do not play any role. When $\langle\rho\rangle\rightarrow\rho_c$, we expect $F\rightarrow0$ since in this limit the kinetic constraints are very effective in slowing down the dynamics and driving the system to a structural arrest [7]. Since no motion is allowed in the limit $F\rightarrow0$, we expect the relaxation time τ to diverge in this limit.

In Fig. 4 we plot the steady-state values of F, averaged over 50 runs, for each value of $\langle\rho\rangle$. We found that F vanishes at a critical density $\rho_c^F=0.471\pm0.005$, with a power-law behavior $120(\rho_c^F-\langle\rho\rangle)^{\gamma_c^F}$, being $\gamma_c^F=4.19$, very close to the value $\gamma_c^F\sim4.7$ obtained in the KA model [7]. In the same figure we also report the values of F for the system size $L=16$. In this case we found that F vanishes with a power-law behavior and the estimated critical density is 0.482 ± 0.016, which is consistent with ρ_c^F within the error range, and no significant lattice size effect. It is interesting to note that $\rho_c^F\simeq\rho_c$, supporting the conclusion that our model shows singular behavior at a density smaller than the maximum possible one, ρ_M. This indicates that LBE with dynamical constraints represents a realizable process.

It is also instructive to define an effective potential energy via the relation

$$V=\frac{-\ln F}{\beta}, \qquad (21)$$

where $\beta=1/c_s^2$ is the inverse temperature (mean-kinetic energy) of the fluid. By definition $V\rightarrow0$ in the diffusive regime
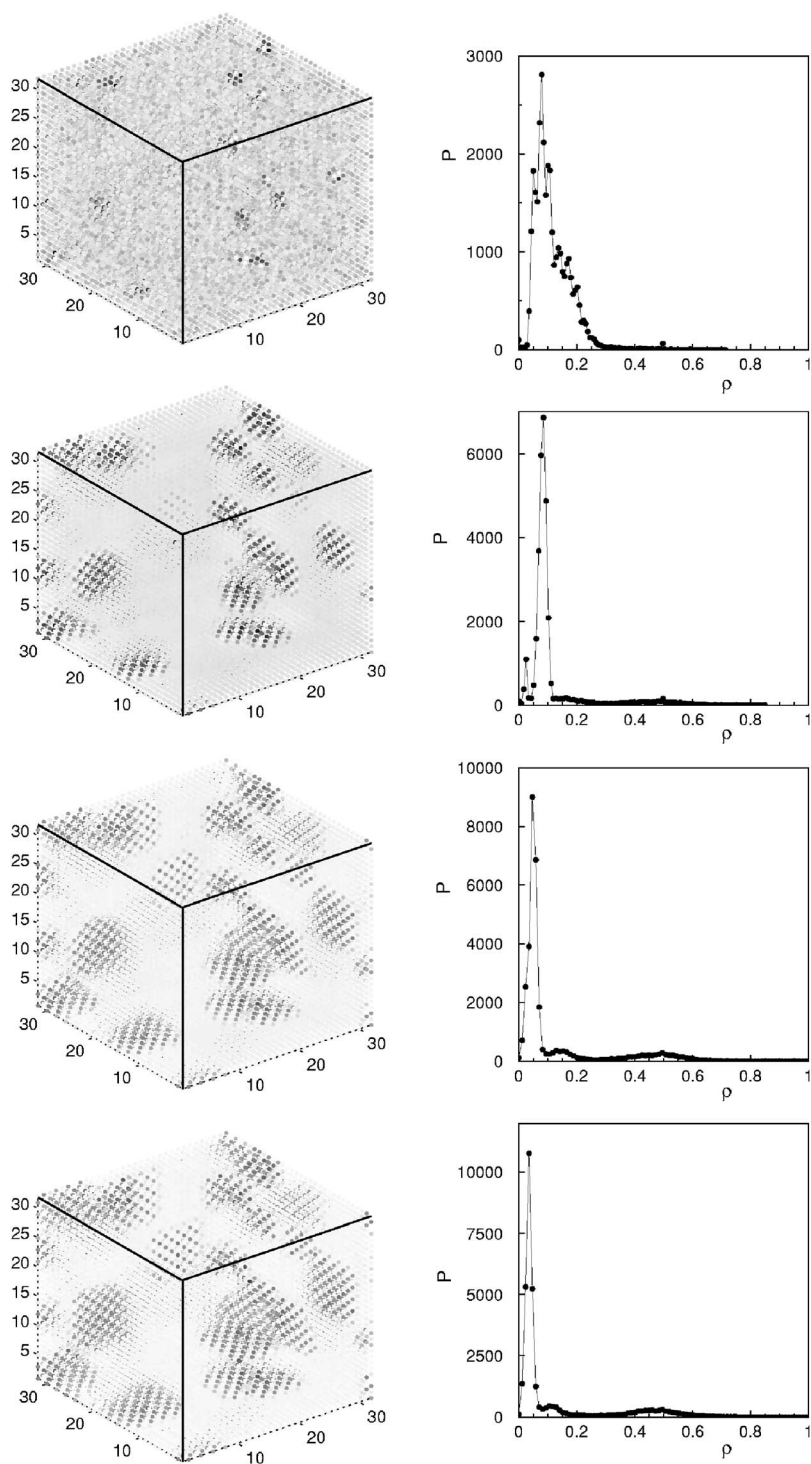
FIG. 5. Configurations (left, gray scaling from white→black corresponds to minimum ρ →maximum ρ) and probability distribution functions (right) at different times (from top to bottom $t=10$, 50, 100, 200) with $\rho_0=0.5$, $\langle\rho\rangle=0.12$, $S=1.5$, and $L=32$.

$(F\rightarrow 1)$, and $V\rightarrow\infty$ in the fully arrested regime $(F\rightarrow 0)$. With this definition, our data show that in the vicinity of the critical threshold $(F\sim 10^{-4})$, the ratio of potential to kinetic energy $\beta V\sim 10$, thus confirming that the fluid is definitely in a strongly-interacting regime, characterized by a dominance of potential over kinetic energy. As discussed in the introduction, such strongly-interacting regime could have not been handled by previous LB models for nonideal fluids.

D. Density configuration and probability distribution

In Fig. 5 we show four snapshots of the density field distribution $\rho(x,y,z;t)$ and the corresponding probability distribution function (PDF) $P(\rho)$, for the case $\rho_0=0.5$, $\langle\rho\rangle=0.12$, $S=1.5$, corresponding to $\lambda=0.48$, marginally within the sluggish regime. In the purely diffusive regime, the initial PDF

$$P(\rho,t=0)=\chi\delta(\rho-\rho_0)+(1-\chi)\delta(\rho), \qquad (22)$$

would evolve irreversibly into a uniform steady state with distribution

$$P_u(\rho,t\rightarrow\infty)=\delta(\rho-\chi\rho_0). \qquad (23)$$
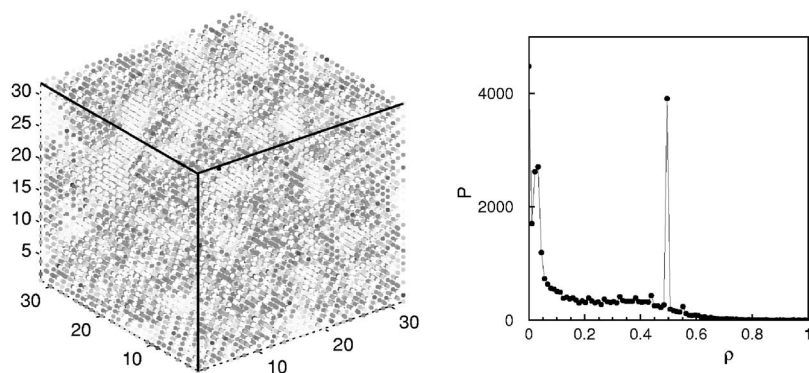
FIG. 6. Configurations (left, gray scaling from white→black corresponds to minimum ρ →maximum ρ) and probability distribution functions (right) in the steady state with $\rho_0=0.5$, $\langle\rho\rangle$ =0.21, $S=1.5$, and $L=32$.

In the weakly-sluggish regime the density PDF shows a strong peak at $\rho\simeq0.05$ with nonetheless a visible remnant of the initial, unthermalized, peaks at $\rho=0,\rho_0$ and a feeble continuum $0<\rho<\rho_{max}$, reaching up to $\rho_{max}\sim1$. The morphology of the density distribution is characterized by a uniform background with a few islands of heterogeneous high-density clusters. Visual inspection of Fig. 5 shows that the morphology of the high-density regions settles down at a relatively early stage of the system dynamics. The situation in the deep sluggish regime, $\rho_0=0.5$, $\langle\rho\rangle=0.21$, $S=1.5$, corresponding to $\lambda=0.84$, is shown in Fig. 6. Two salient features are immediately apparent. First, the unthermalized peaks at $\rho=0$, ρ_0 become dominant, and second, the feeble continuum evolves into a substantial tail bridging the gap between the average and initial values of the density field. This picture confirms the highly non-Gaussian nature of density fluctuations, a well-known feature of dynamically inhomogeneous fluids.

As to morphology, we observe that the high-density regions develop into clusters of smaller size. By moving further into the quasi-arrested regime, $\rho_0=0.5$, $\langle\rho\rangle=0.30$, $S=1.5$, corresponding to $\lambda=1.22$ (see Fig. 7), the density PDF is observed to get closer to the frozen, initial distribution. The density field shows little sign of coherent high-density regions, although some spots of overdense fluid with $\rho>\rho_0$ are still visible. Finally, when entering into the frozen regime ($\lambda\gtrsim1.4$) the system is nearly blocked: The vast majority of the sites stays at density 0 and ρ_0, with only few sites in the range $0\leq\rho\leq\rho_0$, with no specific spatial structure (see next section).

E. Structure factors and cluster size

We have already observed that high-density heterogeneous regions tend to shrink in size as the average fluid den-

sity is increased. This observation can be made more quantitative by computing the spectrum of the density-density correlation (structure function)

$$C(k,t)=\langle\widetilde{\rho}(\mathbf{k},t)\widetilde{\rho}(-\mathbf{k},t)\rangle, \tag{24}$$

where $\widetilde{\rho}(\mathbf{k},t)$ is the spatial Fourier transform of the density fluctuation $\rho(\mathbf{r})-\langle\rho\rangle$ and $k=|\mathbf{k}|$ is the magnitude of the wave vector in Fourier space. The quantity $C(k,t_s)$ at time t_s in the steady state is shown in Fig. 8, for a sequence of increasing values of the average fluid density after averaging over 50 independent runs. At low density, in the purely diffusive regime, a typical exponential decay is observed. As the density is raised, the function $C(k,t_s)$ develops a maximum at finite $k=k_h$, corresponding to the onset of high-density regions, whose size $R\sim2\pi/k_h$ is the typical heterogeneity scale of the system. While approaching the frozen regime, the structure tends to disappear as witnessed by the absence of a peak in the structure factor, that becomes almost flat (see the curve at $\langle\rho\rangle=0.41$ in Fig. 8).

The average size of domains R can be estimated as the inverse of the first moment of the spherically averaged structure factor, that is

$$R=2\pi\frac{\displaystyle\int_0^\pi C(k,t_s)dk}{\displaystyle\int_0^\pi kC(k,t_s)dk}. \tag{25}$$

This quantity is shown in Fig. 9 (data were obtained by averaging over 50 independent runs) as a function of $\rho_c-\langle\rho\rangle$. From this figure, it is seen that by increasing $\langle\rho\rangle$, R decreases from about $R\sim L$ (homogeneous scale) to a minimum R_c of
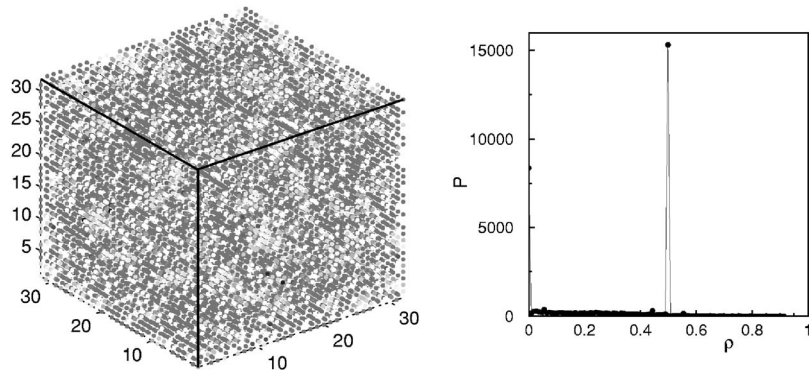
FIG. 7. Configurations (left, gray scaling from white→black corresponds to minimum ρ →maximum ρ) and probability distribution functions (right) in the steady state with $\rho_0=0.5$, $\langle\rho\rangle$ =0.30, $S=1.5$, and $L=32$.
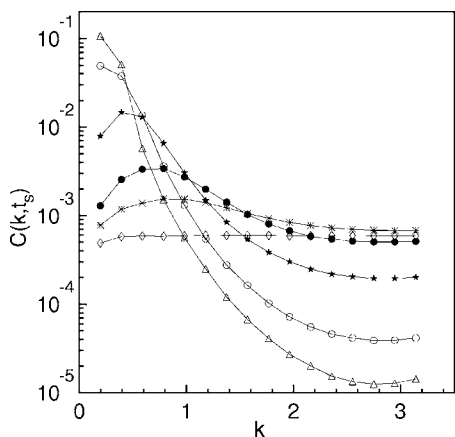
FIG. 8. Spherically averaged structure factor $C(k,t_s)$ as a function of the wave vector k at time t_s in the steady state for $\langle\rho\rangle$ =0.10 ($\triangle$), 0.12 ($\bigcirc$), 0.18 ($\star$), 0.26 ($\bullet$), 0.30 (*), 0.41 ($\diamond$), with ρ_0=0.5, S=1.5, and L=32.

about 4 lattice units. This is the smallest heterogeneity scale the system is able to develop and marks the transition to the frozen regime, where $C(k,t_s)$ is nearly constant.

The same information is conveyed in Fig. 10, where it is the relaxation time τ to be shown as a function of R. It appears that τ goes as $\tau \sim R^{-3/2}$ in the glassy regime (R_c $< R \lesssim 20$) and then exhibits an exceedingly hard divergence as R approaches R_c, reflecting the fact that the system is *defacto* blocked when $\langle\rho\rangle > \rho_c - 0.05$.

IV. COMPUTATIONAL PERFORMANCE

Since all discrete populations at each lattice site move simultaneously and independently of each other, the present LB model can be viewed as an effective one-body KA model, with intrinsic parallel dynamics. As a result, a single time step of the present LB scheme is basically equivalent to $6L^3$ KA steps.

A typical run on a 32^3 lattice (four times larger than typical lattice glass simulations [7,9]) takes just a few minutes on
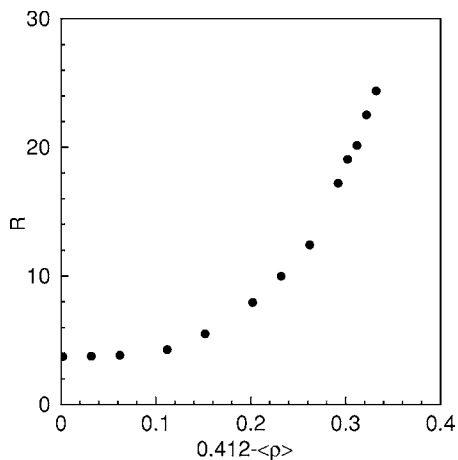
FIG. 9. Average size R of domains in the steady state as a function of $0.412-\langle\rho\rangle$ with ρ_0=0.5, S=1.5, and L=32.
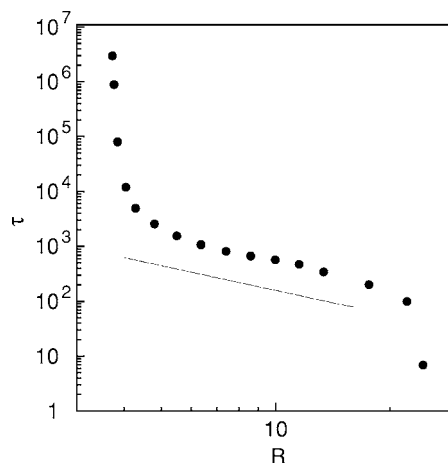
FIG. 10. Relaxation time τ as a function of the average size R with ρ_0=0.5, S=1.5, and L=32. The straight line has slope $-3/2$.

a 2.4 GHz Intel Xeon processor. Of course, this dramatic acceleration comes at the expense of having replaced the many-body KA dynamics with an effective one-body LB dynamics. An undesirable side effect of this replacement is a slight lack of ergodicity, as signaled by the fact that $h(\tau)$ does not decay exactly to zero because the system gets arrested in correlated configurations from which it is unable to escape due to the lack of fluctuations. Further many-body effects possibly lost along the way by the present one-body formulation necessitate further scrutiny.

V. CONCLUSIONS AND FUTURE DEVELOPMENTS

Summarizing, we have introduced an extension of the LB method which includes self-consistent constraints based on the nonlocal density of the surrounding fluid. This LB model with dynamic density constraints proves capable of reproducing *some* typical features of dynamically heterogeneous fluids, such as sluggish relaxation and non-Gaussian density distributions. Due to its intrinsically parallel dynamics, the present mesoscopic model is expected to compute much faster than molecular dynamics, Monte Carlo and lattice glass models. The present LB approach was explicitly designed to convey many-body effects into a set of effective constraints on the one-body particle distributions. As a result, it would be of interest to assess the range of validity of such an approximation as compared with genuinely many-body approaches. As an example, one may want to investigate whether the clusters observed in the present simulations bear any relation, if only an approximate one, with the inherent structures of the multidimensional landscape approach [4]. It would also be worthwhile to explore whether the density threshold S (the only free parameter of our model) can be derived from self-consistent dynamic arguments. Finally, as previously observed, it would be interesting to unravel potential connections of the present LB scheme with mathematical models for granular and traffic flows.

[1] For reviews, see e. g., C. A. Angell, Science **267**, 1924 (1995); H. Sillescu, J. Non-Cryst. Solids **243**, 81 (1999); S. C. Glotzer, J. Non-Cryst. Solids **274**, 342 (2000); P. G. Debenedetti and F. H. Stillinger, Nature (London) **410**, 259 (2001).

[2] J. P. Garrahan and D. Chandler, Phys. Rev. Lett. **89**, 035704 (2002).

[3] U. Bengtzelius, W. Götze, and A. Sjölander, J. Phys. C **17**, 5915 (1984); E. Leutheusser, Phys. Rev. A **29**, 2765 (1984).

[4] T. S. Grigera, A. Cavagna, I. Giardina, and G. Parisi, Phys. Rev. Lett. **88**, 055502 (2002); M. S. Shell, P. G. Debenedetti, E. La Nave, and F. Sciortino, J. Chem. Phys. **118**, 8821 (2003).

[5] W. Kob and H. C. Andersen, Phys. Rev. Lett. **73**, 1376 (1994).

[6] K. Binder, J. Baschnagel, and W. Paul, Prog. Polym. Sci. **28**, 115 (2003); for a reference on numerical methods see, e.g., M. P. Allen and D. J. Tildesley, *Computer Simulation of Liquids* (Clarendon Press, Oxford, 1987).

[7] W. Kob and H. C. Andersen, Phys. Rev. E **48**, 4364 (1993).

[8] G. Biroli and M. Mezard, Phys. Rev. Lett. **88**, 025501 (2002).

[9] M. P. Ciamarra, M. Tarzia, A. de Candia, and A. Coniglio, Phys. Rev. E **67**, 057105 (2003); **68**, 066111 (2003).

[10] F. Ritort and P. Sollich, Adv. Phys. **52**, 219 (2003).

[11] C. Toninelli, G. Biroli, and D. S. Fisher, Phys. Rev. Lett. **92**, 185504 (2004).

[12] E. Bertin, J.-P. Bouchaud, and F. Lequeux, Phys. Rev. Lett. **95**, 015702 (2005).

[13] J. K. Percus, Mol. Phys. **100**, 2417 (2002).

[14] F. Higuera, S. Succi, and R. Benzi, Europhys. Lett. **9**, 345 (1989).

[15] R. Benzi, S. Succi, and M. Vergassola, Phys. Rep. **222**, 145 (1992); D. A. Wolf-Gladrow, *Lattice Gas Cellular Automata and Lattice Boltzmann Models* (Springer-Verlag, New York, 2000).

[16] M. R. Swift, W. R. Osborn, and J. M. Yeomans, Phys. Rev. Lett. **75**, 830 (1995); A. Lamura, G. Gonnella, and J. M. Yeomans, Europhys. Lett. **45**, 314 (1999); T. Ladd, J. Fluid Mech. **271**, 285 (1994).

[17] A. Lamura and S. Succi, Eur. Phys. J. B **39**, 241 (2004); Physica A **325**, 477 (2003); Int. J. Mod. Phys. B **17**, 145 (2003).

[18] A. Lamura and S. Succi, Phys. Rev. Lett. **95**, 224502 (2005).

[19] M. D. Ediger, Annu. Rev. Phys. Chem. **51**, 99 (2000).

[20] P. Bhatnagar, E. P. Gross, and M. K. Krook, Phys. Rev. **94**, 511 (1954).

[21] Y. H. Qian, D. d'Humieres, and P. Lallemand, Europhys. Lett. **17**, 479 (1992).

[22] I. Rasin, S. Succi, and W. Miller, J. Comput. Phys. **206**, 453 (2005).

[23] X. Shan and H. Chen, Phys. Rev. E **47**, 1815 (1993); **49**, 2941 (1994).

[24] J. Jäckle, Rep. Prog. Phys. **49**, 171 (1986).

[25] W. Kob (private communication); for a comparison between MCT and real systems see, e.g., W. Götze and J. Sjögren, Rep. Prog. Phys. **55**, 241 (1992).